Anisotropy effects in physical sputtering investigated by laser-induced fluorescence spectroscopy

A. Goehlich, N. Niemöller, and H. F. Döbele
Institut für Laser- und Plasmaphysik, Universität Essen, Universitätsstraße 2-5, D-45117 Essen, Germany
(Received 24 April 2000)

We report in this article on experimental investigations of angle and energy dependencies of energy spectra of sputtered metal atoms and on deviations from linear cascade theory (Sigmund-Thompson model). Tungsten and titanium targets are bombarded by noble gas ions in the energy range between 0.2–5 keV. Energy distributions have been determined by laser-induced fluorescence spectroscopy with scanning of narrow bandwidth dye laser radiation over the Doppler broadened absorption. The geometry adopted makes it possible to vary both the angle of observation of the sputtered particles and the angle of incidence of the projectiles independently of each other. The observed differences to the theory mentioned are compared both with analytical models and with TRIM.SP–Monte Carlo simulations. The influence of direct recoil atoms on the energy spectrum is discussed in particular.

I. INTRODUCTION

Physical sputtering is finding widespread application in important technical and scientific processes: It is the basis of particle sources in thin film deposition and is applied for surface modification[1] and analysis [SIMS and SNMS (Ref. 2)]. The properties of modified surfaces and the generated layers are sensitively dependent on the energy and angular distribution of the impinging particles.

Another example where sputtering is important is plasma-wall interaction in fusion research: the bombardment of the confining inner wall of a reactor (divertor plates or limiter) by energetic particles leads to a release of atoms and molecules which can penetrate the plasma. These will, after ionization, radiate bremsstrahlung and line radiation which leads to cooling of the plasma.[3] Various approaches have been considered to minimize these losses. One consists in the use of low-Z wall materials, since in this case the number of possible ionization stages is small and the radiation losses are reduced accordingly. There are, however, also concepts based on the use of high-Z materials like tungsten, because of its high sputtering threshold and the favorable redeposition and thermal properties.[4,5] The penetration depth in the plasma of the released impurities is determined by their velocities. It is, therefore, important to have a thorough understanding of the velocity distribution of the impurities and its dependence on the projectile energy and incident angle and to be able to describe by simulations the ongoing processes as reliably as possible.

The dominant fraction of sputtered particles is released as neutrals.[6] Laser-based methods are therefore particularly well suited to their detection. There exists, however, only a very limited number of contributions where angular dependencies of velocity distributions of sputtered particles were investigated. Berres und Bay[7] used a cw-dye laser to study sputtered circonium atoms under two different geometries—the forward and backward scattering directions. The geometry adopted did not allow them, however, to vary systematically the angle of observation independently of the chosen angle of incidence. Another important contribution to this topic is the EARN experiment (energy and angle resolved neutral analysis) by Winograd and co-workers.[8] Laser post-ionization is combined with a time-of-flight measurement and detection by a particle detector with spatial resolution to yield the angular resolution. The angle of emission is found on the basis of a nonlinear transformation from the position where the particle is detected at the multichannel plate detector. We describe in this paper an experiment based on pulsed laser induced fluorescence diagnostics at a specially designed vacuum chamber which allows the selection of combinations of angles of incidence and observation. Laser induced fluorescence has the disadvantage—as compared to laser post ionization—to be less sensitive so that ion sources with higher fluxes are required to generate high enough particle densities and the domain of application is therefore restricted. It has, however, the advantage that the measured Doppler broadened spectra are directly linked to the velocity distribution of the released particles.

II. THE ISOTROPIC THEORY

Thompson[9,10] and Sigmund[11–13] have published several basic papers on physical sputtering. Thompson arrived at an expression for the energy distribution of sputtered particles on the basis of fundamental physical assumptions. The main assumption is the generation of extended isotropic recoil cascades of low-energy recoil atoms by an isotropic source of energetic primary recoil particles. A binary interaction described by a power-law dependence is a reasonable assumption for not too small collision energies. This power law is approximated from the Thomas-Fermi potential and is of the form $V(R) \propto R^{-1/m}$. This potential leads, according to Lindhard, to a collision cross section which reads $d\sigma = C_m E^{-m} T^{-1-m}$, where E is the energy of the colliding ion, T is the transferred energy, and C_m is a constant. The exponent m depends in principle on the bombarding energy and assumes values between zero and one $(0<m<1)$.[14] The analytical form of this cross section has simple scaling properties and allows analytical solutions in transport theory.[11] For low collision energies around several eV strong screening of the Coulomb potential occurs, and values of m close to zero have to be adopted.

The resulting energy distribution of the sputtered particle flux in the isotropic limit Γ_{iso} is determined by the height E_b of the (planar) surface potential and the maximum transferable energy T_m:[10]

$$\Gamma_{\mathrm{iso}}(E,\theta)dE\,d\Omega \propto \frac{E}{(E+E_b)^{3-2m}} \times\left[1-\left(\frac{E+E_b}{T_m}\right)^{1-m}\right]\cos\theta\,dE\,d\Omega$$

with

$$T_m=\gamma E_0=\frac{4M_1M_2}{(M_1+M_2)^2}E_0. \tag{1a}$$

θ denotes the polar angle of emission with respect to the outer surface normal, and E_0 is the energy of the projectile. M_1, M_2 are the mass of the projectile and target atom, respectively. The energy distribution as given above exhibits a falloff towards higher energy as E^{-2+2m} (for $E_b \ll E \ll T_m$), and exhibits—as physically required—a cutoff at the maximum transferable energy T_m. The assumption of an isotropic momentum distribution underlying Eq. (1a) is not justified for emission energies near T_m, however. If emission energies small compared to the maximum transferable energy T_m and hard collisions ($m \approx 0$) are considered, the so-called Thompson energy spectrum is obtained from Eq. (1a):

$$\Gamma_{\mathrm{iso}}(E,\theta)dE\,d\Omega \propto \frac{E}{(E+E_b)^3}\cos\theta\,dE\,d\Omega. \tag{1b}$$

This result was also obtained by Sigmund as the leading order of an asymptotic expansion in a transport equation treatment.[12,13] The energy distribution of physically sputtered particles according Eq. (1b) peaks at $E_b/2$ and exhibits a characteristic falloff towards high energies as E^{-2}. If the penetration depth of the impinging ion (typically some nm for average mass ions) is much larger than the typical depth of origin of the sputtered particles (typically of the order of a monolayer), the motion of the projectile is decoupled from the motion of the recoil atoms which lead to the emission of atoms through collisions near the surface. The energy distribution is then independent of the mass, the energy and the direction of the projectiles (limiting case of complete isotropy). The energy distribution is in particular independent of the direction of emission for atoms which are ejected with small energies, because the condition of an isotropic momentum distribution is more easily fulfilled for these atoms.

III. ANISOTROPY CORRECTIONS

Momentum conservation causes a conflict between the assumption of an isotropic velocity distribution of recoiling atoms in the solid and the highly directional motion of the bombarding projectile.[15] Anisotropy corrections of the recoil flux density Γ were calculated in the limiting case $E \ll E_0$ as a series of powers of E/E_0 from the asymptotic solution of a set of transport equations.[16,17] It was shown that the leading anisotropic correction can be decomposed in two terms depending on the deposited momentum and the gradient of the deposited energy distribution.

If inelastic energy losses are neglected, the transport equation treatment yields for an infinite scattering medium an expression for the flux distribution of recoiling atoms.[16] The treatment of a bounded medium is discussed, e.g., in Ref. 18). Backward sputtering corresponds to the flux taken at the surface. Allowing for surface refraction at a planar surface potential the following expression for the energy distribution of the backsputtered particle flux is obtained:

$$\Gamma(E,\theta,\chi)\propto\Gamma_{\mathrm{iso}}(E,\theta)\Big(1+\alpha_x\sqrt{E\cos\theta^2+E_b} +\alpha_y\sqrt{E}\sin\theta\cos\chi +\beta\sqrt{E\cos\theta^2+E_b}\frac{\sqrt{E+E_b}}{NS(E+E_b)}\Big)$$

with

$$\alpha_x=\frac{-3F^0_{p,x}(E_0,\mathbf{e},0)}{\sqrt{2M_2}F_D(E_0,\mathbf{e},0)},\quad \alpha_y=\frac{3F^0_{p,y}(E_0,\mathbf{e},0)}{\sqrt{2M_2}F_D(E_0,\mathbf{e},0)}, \tag{2}$$
$$\beta=K_m\frac{\frac{\partial}{\partial x}F_D(E_0,\mathbf{e},x)_{x=0}}{F_D(E_0,\mathbf{e},0)}.$$

It is assumed here that the positive x axis (depth coordinate) is parallel to the inner target normal and that the incident beam is located within the xy plane ($x=0$ describes the position of the source). χ denotes the azimuthal angle of emission. $\mathbf{e}$ describes the direction of the incoming ion. $S(E)$ denotes the nuclear stopping power[11] and N is the target atom density. In the formulation given above the scattering power m enters explicitely only through the constant K_m (for exact definition of K_m, see original literature[16]).

$F_D(E_0,\mathbf{e},x)$ is the distribution of energy deposited at the surface. The statistical distribution $\mathbf{F}^0_P(E_0,\mathbf{e},x)$ is linked to the deposited momentum density.[19,20] This function has an azimuthal symmetry with respect to the beam direction $\mathbf{e}$. The statistical distributions can be obtained explicetely by solution of separate transport equations[16,19,20] or by Monte Carlo simulation.[21,22]

The quantity α_x in Eq. (2) is usually positive, since the x component of the deposited momentum density is directed outward at the surface.[20] α_y equals zero for normal incidence for reasons of symmetry.

The last term in Eq. (2) is proportional to the gradient of the deposited energy and is symmetric with respect to the surface normal. It describes a particle flux proportional to the gradient of the deposited energy profile in analogy to a diffusion current.

The contribution to the anisotropy correction due to the gradient term is dominant for large ratios of energies of the projectile to the recoil atom energy [e.g., $E_0/E \gg 0.01$ (Ref. 16)] and leads in comparison to the isotropic spectrum [Eq. (1b)] to a broadening and a peak shift towards higher emission energies for normal emission; the energy distribution narrows and the peak shifts back towards smaller energies for oblique emission angles. However, only weak dependencies on the emission angle are introduced in this case. The contribution of the momentum term scales according to

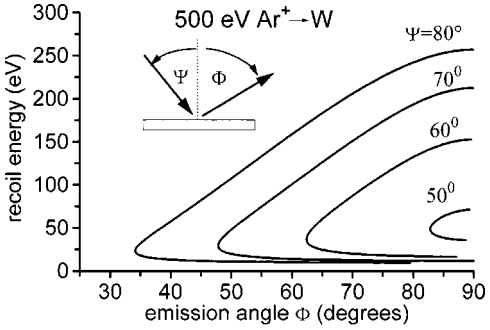

FIG. 1. Energy of a direct recoil atom (tungsten) versus emission angle. Surface refraction due to a planar surface potential is applied.

$\sqrt{M_1E/M_2E_0}$ and is expected to become more important with falling impact energies E_0. The momentum term causes similar changes to the spectrum as the gradient term for normal incidence. In case of oblique incidence an additional broadening of the energy distribution and a shift of the maximum of the energy distribution towards higher energies occurs ($\alpha_y>0$), if the emission is observed in forward direction. Since the solution of the transport equation is based on the leading orders of a high energy expansion, its applicability is limited to the high energy bombardment case (some keV, say), however.

Computer simulations like the well known Monte Carlo code TRIM.SP (Ref. 23) are well suited, alternatively to analytic approaches and numerical solutions of the Boltzmann equation,[24] to calculate angular dependencies of the yield and energy distributions. Binary collisions are modeled by a screened Coulomb potential, e.g., the krypton-carbon (KrC) or the universal potential.[23] The limitations of the TRIM.SP code towards small bombarding energies are mostly due to the importance of multiple interactions. Provision is made in TRIM.SP for an approximate treatment of weak simultanous collisions, by searching further target atoms in additional collision cylinders. This treatment can be regarded as an approximation to multiple collisions.[23] Further assumptions concerning the applicability are the amorphous structure of the solid, corresponding for a polycrystalline target to an average over many crystallites and a surface which is atomically rough.[23]

IV. THE INFLUENCE OF DIRECT RECOILS

For the case of oblique incidence there is a contribution of direct recoil atoms to the anisotropy of the energy distribution.[25,26] We will limit here the discussion to elastic collisions and consider the emission in the polar plane, i.e., the plane that contains both the target normal and the direction of incidence. The emission angle in the polar plane is denoted in the following by Φ and is measured with respect to the (outer) target normal ($\Phi>0$ for emission on the side opposite to the beam direction; see Fig. 1). For certain angular regions in forward direction it is possible that a target atom located initially close to the surface is ejected as consequence of a single collision with a projectile (mass M_1, energy E_0). The energy transferred to a target atom of mass M_2 initially at rest is then

$$T=\gamma E_0(\cos\varphi)^2. \tag{3a}$$

φ is the recoil angle of the target atom with respect to the direction of the impinging projectile ($0<\varphi<\pi/2$). With Ψ and Φ_0 indicating the angles of incidence and emission (inside the solid) with respect to the target normal, we find

$$\varphi=\pi-\Phi_0-\Psi. \tag{3b}$$

The possible angles of emission Φ_0 are restricted to the interval $\pi/2-\Psi<\Phi_0<\pi/2$.

For not too large energies of the ejected atoms the angle of emission is significantly influenced by the surface barrier of the solid. For an ideally plane surface of potential height E_B the atom is refracted away from the surface normal in analogy to Snell's law in optics. Conservation of energy and momentum connects the internal angle Φ_0 and the external angle Φ:[11]

$$(T-E_b)(\cos\Phi)^2+E_b=T(\cos\Phi_0)^2. \tag{4}$$

Substituting the transferred energy T from Eqs. (3a) and (3b) yields

$$\cos(\Phi)^2=\frac{\cos(\Phi_0+\Psi)^2\cos(\Phi_0)^2-\epsilon}{\cos(\Phi_0+\Psi)^2-\epsilon},$$

with

$$\epsilon=\frac{E_b}{\gamma E_0}. \tag{5a}$$

The energy $E_{\rm rec}$ of the direct recoil atom is then given by

$$E_{\rm rec}=\gamma E_0\cos(\Phi_0+\Psi)^2-E_b. \tag{5b}$$

This allows to represent the energy of the sputtered direct recoil atom as a function of the emission angle Φ. Figure 1 shows the dependence of the direct recoil energy on the emission angle for a fixed projectile energy (500 eV and $Ar^+\rightarrow W$). Note that direct emission is only possible for a limited range of angles of incidence.

There are two branches which coincide at a ''critical'' angle of emission. Beyond this angle there are two possible recoil energies corresponding to collisions with different impact parameters but leading to the same emission angle. The low energy branch corresponds to collisions with a large impact parameter (e.g., $\varphi\approx\pi/2$) and correspondingly small energy transfer T to the target atom. If T is of the order of the surface binding energy, the influence of the latter becomes important with the result that, due to the increasing value of the scattering cross section with decreasing T the emission becomes more efficient as compared to the high energy branch (collisions with large energy transfer). These low energy recoil atoms lead to a broadening and a shift of the maximum of the energy distribution in the considered angular interval. It should not be overlooked, however, that there is also an influence of multiple interactions for low energy collisions, as well as inelastic energy losses and effects caused by surface roughness. This latter influence leads to a smearing out of the direct recoil energies particularly in the vicinity of the critical angle $\Phi_{\rm crit}$, where the recoil energy $E_{\rm rec}$ is a strong function of the emission angle. The high energy branch is generated by fast atoms which are only

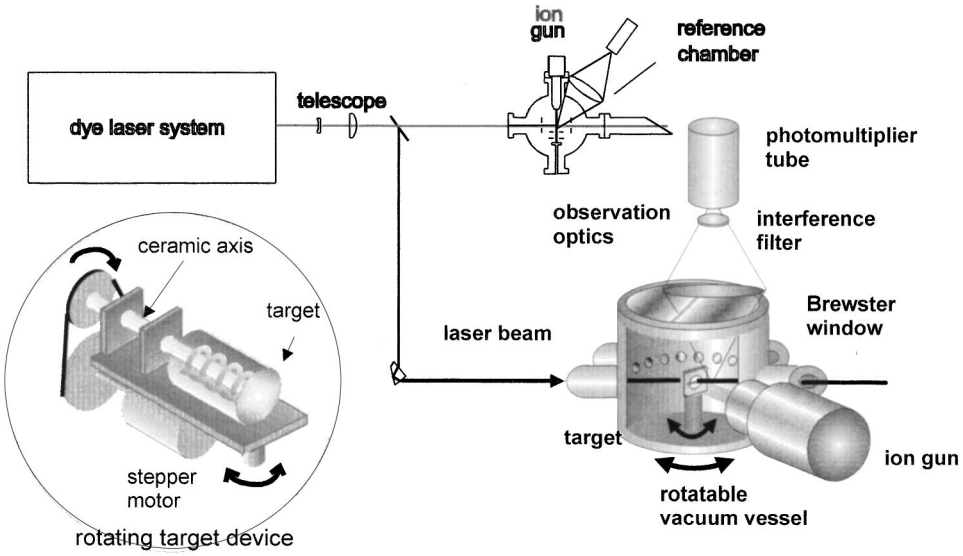

FIG. 2. Sketch of the experimental setup. The inset depicts an optional specially designed target mount which allows rotation during sputtering. The standard mount with a slit is drawn inside the rotatable vacuum vessel.

weakly influenced by surface refraction. It is therefore close to the uncorrected curve according to Eqs. (3a) and (3b). Isolated ''direct recoil peaks'' are only expected for angles much larger than the critical angle.

V. EXPERIMENT

The experimental setup is shown in Fig. 2. Polycrystalline pure metal targets (ALFA Products), polished to optical quality with 1 μm diamond powder, are cleaned prior to a measurement by bombardment with the ion beam generated by a 1 cm Kaufmann source (CSC). A system of apertures in front of the target limits the ion beam diameter to 10 mm. Typical current densities are between 100 and 500 μA/cm^2 for bombardment energies between 200 and 500 eV. In few cases measurements at 5 keV were carried out. The Kaufmann ion source was exchanged for this purpose against a cold cathode ion gun (Fisons AG5000). Two different target mounts (I and II in the following) have been used. The majority of measurements described below was obtained with variant I. The target foils are fixed in this case in a stainless steel holder with a slit through which the laser beam propagates. A stainless steel mask allows a free diameter of the target of 8 mm. The target can be heated by a heating element (Boralectric) to approx. 400 °C. The observed scattering volume is typically located 20–30 mm in front of the target surface.

Target mount II—see inset in Fig. 2—allows for rotation of the target during bombardment with respect to the target normal in order to prevent the generation of a surface topography with preferential directions.[27] The target—a circular foil in this case—is mounted on the front side of a metal cylinder, 13 mm in diameter, supported by a ceramic axis. This cylinder can be heated up to about 600 °C with a tungsten filament. The laser beam passes the rotating cylinder closely above its upper circumference in this case. The scattering volume is located approximately 40 mm in front of the target surface in order to minimize geometrical corrections regarding the finite extension of the target and the slight off-axis arrangement. The whole target mount can be rotated in the polar plane with the aid of a stepping motor driven gear box under vacuum in order to select a specific angle of incidence. The vacuum chamber is equipped with 15 viton-sealed suprasil laser windows, 20° apart on the circumference. The chamber (base pressure 2×10^{-8} mbar) and the attached turbo pump are connected to the roughing pump through a bellows which allows a rotation angle of up to 270°. Since the position of the observation volume is fixed through the observation optics (attached to main experimental table), rotation of the chamber permits to choose a specified angle of emission.

The sputtered atoms are excited by a pulsed (~15 ns) UV laser beam generated by an excimer laser-pumped dye laser with a frequency doubling stage (Lamda Physik EMG 200+FL 2002). The excitation of ground state tungsten atoms is performed by radiation at $\lambda\simeq291.1$ nm [corresponding to an unclassified state at 34 342 cm^{-1} (Ref. 28)]. The fluorescence light at $\lambda\simeq403$ nm (life time $A^{-1}=93$ ns) is detected with a photomultiplier (Hamamatsu R928) through an interference filter (FWHM=5 nm). Ground state titanium atoms are detected with excitation at $\lambda\simeq294.2$ nm and observation around $\lambda\simeq445$ nm. This excitation scheme was also used earlier by Dullni.[29] The photomultiplier signals are accumulated with a boxcar averager (Stanford Research SR250) and are analyzed by a computer.

The fact that the velocity distribution is unsymmetric (since all sputtered atoms move away from the surface) requires an accurate spectral calibration of the zero velocity spectral position. This is realized by a fluorescence setup operating in parallel in a separate chamber; the atoms are again generated by ion beam sputtering. The optical excitation is performed in this case perpendicular to the direction of particle emission so that a spectrally symmetric profile results. The spectral position of the maximum yields the zero velocity position of the first fluorescence setup. Both the fluorescence signals from the main experiment and from the zero velocity calibration setup are stored simultaneously. Furthermore, a small fraction of the laser beam is separated by a beam splitter for normalizing purposes.

Absorption profiles determined by laser induced fluorescence are known to be subject to nonlinear distortion effects at higher pump powers due to saturation.[30] In order to exclude or minimize these effects, the intensity of the laser

pulse is attenuated to approach the linear section of the saturation curve.

For the operation of the ion source the chamber is filled to typically 5×10^{-5} mbar with a noble gas. The scanning of the fluorescence transition is performed by tuning the laser over the Doppler-broadened resonance with aid of a homemade, stepper motor controlled pressure scanning unit. The laser linewidth (narrowed by an intracavity etalon) allows us a velocity resolution of approximately 0.7 km/s. The spectral position is monitored simultaneously with a monitor etalon.

Between 10 to 100 fluorescence pulses are summed up—depending on the signal amplitudes. The velocity of the atoms which are excited at a fixed setting of the pressure P in the sealed dye laser oscillator chamber is calculated from the difference $P-P_0$ (P_0: pressure at the maximum of the reference line), the pressure interval P_{FSR} between two consecutive peaks of the interference pattern obtained with the monitor etalon, the frequency of the transition ν_0 and the free spectral range ν_{FSR} of the etalon:

$$v=c\,\frac{\nu_{\mathrm{FSR}}}{\nu_0}\,\frac{(P-P_0)}{P_{\mathrm{FSR}}}.$$

The measured velocity-density-distributions $n(v)$ allow us to calculate the energy distribution of the sputtered flux:

$$f(E)=v\,n(v)\,\frac{dv}{dE}\propto n(\sqrt{2E/M}).$$

[The LIF signal is proportional to the number density in the scattering volume (dimension along the beam direction: $\Delta L=5$ mm typically) for resting particles. A possible correction due to the motion of atoms in or out of the scattering volume is negligible as long as $v\tau\ll\Delta L$ (τ denotes the time of measurement—typically of the order of the lifetime). For Ti this condition is uncritical due to the short lifetime of the upper state ($A^{-1}\sim4$ ns). For tungsten the lifetime is about 93 ns. It can be shown that velocity dependent contributions of the detection probability cancel, however. The relative emission probability of a photon within a time t after an infinitisimal ''short'' excitation is given by $P(t)=1-e^{-At}$. Then the number of detected photons S is proportional:

$$S\propto(\Delta L-v\tau)P(\tau)+\int_0^{v\tau}dx P\left(\frac{x}{v}\right)+\int_0^{v\tau}dx e^{-Ax/v}P\left(\tau-\frac{x}{v}\right).$$

The first term is due to atoms which stay in the scattering volume during the registration time, the second contribution is due to atoms which leave the volume, and the last term is due to excited atoms which enter the scattering volume. Inserting the aforementioned probability $P(t)$ yields $S\propto\Delta L P(\tau)$. The result is the same for particles at rest.]

RESULTS AND DISCUSSION

Figures 3(a)–3(d) show experimental energy distributions of sputtered tungsten atoms (cubes) for bombarding energies of 5000, 500, 300, and 225 eV for a fixed geometry: normal incidence and normal emission. Shown for comparison are also the Thompson distribution [Eq. (1b), dashed] calculated with a surface binding energy of $E_b=8.7$ eV corresponding to the sublimation heat.[31] The step functions shown are results of Monte Carlo calculations using the TRIM.SP (ver. TRVMC95) code.[23] The simulations are based on the KrC-interaction potential, and the heat of sublimation has been used for the surface binding energy. A 50:50 mixture of the nonlocal Lindhard-Scharff and the local Oen-Robinson stopping power was adopted for the inelastic electronic loss.[23] The experimental distribution, Fig. 3(a), is well approximated for a bombarding energy of 5 keV by a Thompson distribution describing the isotropic limiting case with a high energy tail corresponding to E^{-2}. Note also the good agreement with the TRIM.SP result. The experimental distribution exhibits, however, a slight shift of the maximum towards higher energy. If we consider E_b in a more general sense as a formal fitting parameter to describe the distribution, one arrives after minor corrections for the geometry (see Ref. 32) and after convolution with the laser profile at a value of $E_b=10$ eV. For smaller bombarding energies the tails of the spectra exhibit clear deviations when compared to the reference distribution Eq. (1b) [Figs. 3(c)–3(d)]. This steeper slope of the measured distributions at higher energies of the sputtered atoms for the case of bombardment with low energy ions is in agreement with earlier results[33] and also with the results of the simulation calculations. It could be explained qualitatively by the higher energy loss in low energy collisions: the projectile is deflected by large angles at low collision energies and is slowed down with large energy loss thus generating collision cascades of only rather limited size. This situation is better described by the ''single knock on'' regime of sputtering.[11] The mass ratio is, in addition, very unfavorable for the case of sputtering of tungsten atoms by argon ions so that a comparatively small amount of energy is transferred for generating recoil cascades. Primary recoil atoms generated by ions reflected inside the solid are, however, important in this case. The theory formulated by Falcone[34,35] for bombardment with light projectiles takes this sputtering mechanism into account; the calculated energy distributions are tentatively included for comparison in Figs. 3(b)–3(d). This distribution (which yields a better approximation to our results) is of the form

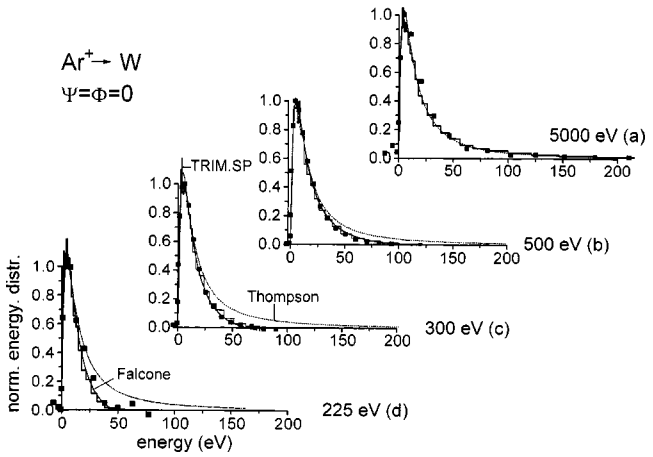

FIG. 3. (a)–(d) Dependence of the energy distribution of sputtered tungsten atoms for fixed geometry (normal incidence and emission) on the bombarding energy. The TRIM simulation is shown as a step function together with the Thompson distribution as a reference (dashed line). In (b)–(d) also the light ion sputtering theory according to Falcone is shown.

$$\Gamma(E) \propto \frac{E}{(E+E_b)^{5/2}} \ln\left(\frac{E_c}{E+E_b}\right) \quad (E+E_b<E_c). \quad (6a)$$

The ''cutoff'' energy E_c in this distribution has been identified with the maximum energy which can be transferred to a target atom by a *reflected* projectile, namely

$$E_c = \gamma(\gamma-1)E_0. \quad (6b)$$

The dependence of the energy distributions on the angle of emission at normal incidence is only weak for sputtered tungsten atoms. No significant change was observed in case of the bombardment of tungsten with 500 eV argon ions for angle variations from $\Phi=0°$ to $\Phi=60°$. We do not show the data here for this reason. A more significant angular dependence of the energy distributions for normal incidence was found in contrast for high collisional energy transfer, e.g., the nearly equal mass case: bombardment of titanium with argon ions. The anisotropy is increasing as expected with falling impact energy as demonstrated in Figs. 4(a)–4(c), where energy distributions at normal ($\Phi=0°$) and oblique incidence ($\Phi=60°$) are compared for different bombarding energies.

In order to describe the angular variation of the energy distributions by a simple analytical formula we use the form suggested by the momentum term Eq. (2):

$$\Gamma(E,\Phi) \propto \frac{E}{(E+E_b)^3}(1+\lambda\sqrt{E\cos\Phi^2+E_b}). \quad (7a)$$

λ is treated here as an empirical fitting parameter, and Eq. (7a) is considered as meaningful only for positive values. The surface binding energy was inserted according to the heat of sublimation.

This expression corresponds to the first order term in an expansion of the internal energy spectrum in Legendre polynoms of the directional cosine. The amplitude of the correction term is also chosen proportional to the momentum of the recoil atom. The fitting parameter turns out, however, to become negative for low energy bombardment in order to approximate the experimental distributions—indicating a negative correction to the isotropic flux—and should therefore not be interpreted as the deposited momentum density, which would lead to a positive correction. Since Eq. (2) is valid for higher bombarding energies, this is not in contradiction to our data, however.

It is noteworthy that Eq. (7a) describes the angular variation of the experimental data over a broad angular range (with the same fitting parameter λ).

At higher bombarding energy ($E_0=5000\,\mathrm{eV}$) the energy spectra broadens and the fitting parameter becomes positive. The energy distribution is very close to the isotropic spectrum [Eq. (1b)] in this case.

A series of normalized energy distributions for bombardment at $E_0=300\,\mathrm{eV}$ is depicted in Fig. 5 together with the results of the TRIM.SP calculation. The Thompson distribution [Eq. (1b) calculated with the heat of sublimation $E_b=4.9\,\mathrm{eV}$ (Ref. 31)] is also shown for reference (dashed line). For normal emission the experimental distribution is close to the Monte Carlo simulation. The energy distribution again exhibits a deficit of fast particles as compared to the Thompson-distribution. With increasing exit angle the energy distribution broadens and the peak shifts towards higher energies (e.g., for normal emission the distribution peaks at about $E=1.7\,\mathrm{eV}$, while the distribution peaks near $E=3\,\mathrm{eV}$ for emission at $\Phi=60°$–see inset) and the high energy falloff becomes weaker. The simulated distributions exhibit the same trend as the measured distributions at medium emission angles, but their broadening is less pronounced. The broadening of the energy distribution and the peak shift for oblique emission angles is explained qualitatively by single-kock on sputtering by primary recoil atoms, which effectively transfer momentum to surface near atoms (e.g., within a monolayer distance[6]) predominantly at small angles with respect to the surface, thus leading to energetic sputtered particles at oblique emission angles and an ''undercosine'' angular distribution. The most pronounced disagreement between simulation and measurement is found at grazing emission ($\Phi=80°$): whereas the calculated energy distribution exhibits narrowing, the experimental data points are closer to the isotropic Thompson energy spectrum. The influence of the roughness of our ''real'' target surface should be considered here as a possible reason, which is

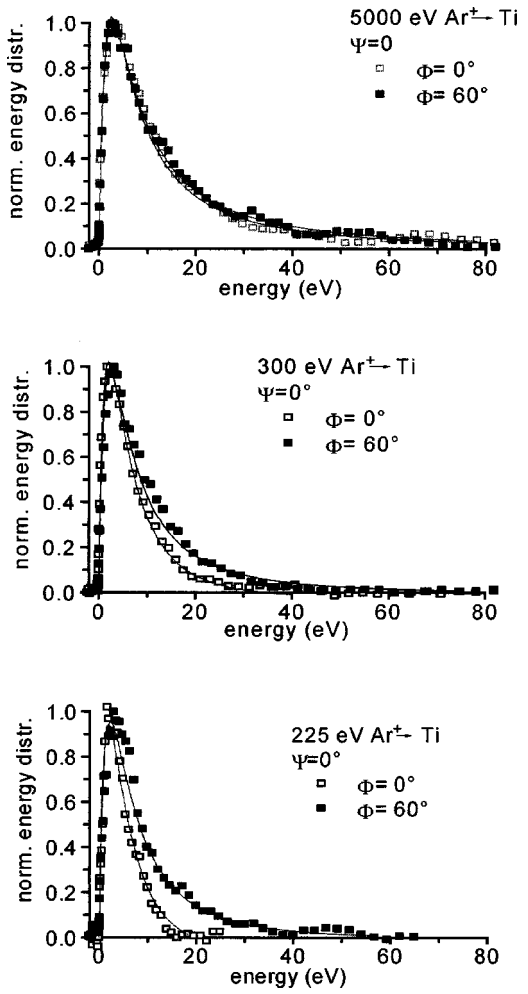

FIG. 4. Anisotropy effect of the energy distributions of sputtered titanium atoms bombarded by 5000 eV, 300 eV, and 225 eV argon ions at perpendicular incidence, shown for normal (open symbols) and oblique emission $\Phi=60°$ (solid symbols). The solid lines are calculated according to Eq. (7a) with $E_b=4.9\,\mathrm{eV}$ and λ is fitted for the normal emission direction ($\lambda=0.13$, -0.16, and -0.2 for $E_0=5000\,\mathrm{eV}$, 300 eV, and 225 eV).

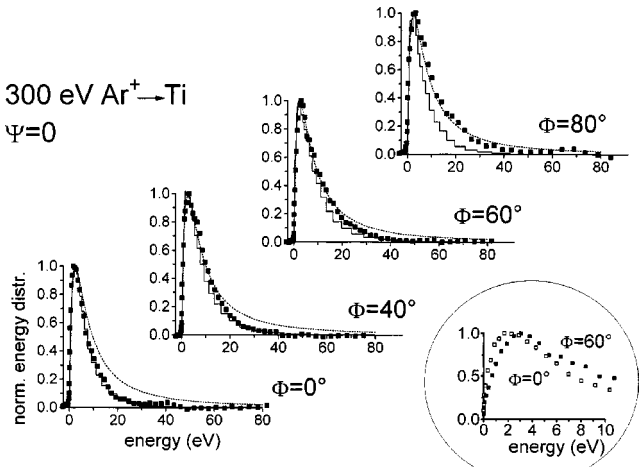

FIG. 5. Comparison of the experimental spectra at perpendicular incidence with the TRIM.SP calculation (shown for various emission angles). The solid line depicts the Thompson distribution [Eq. (1b)]. The peak shift at oblique emission is depicted in the inset.

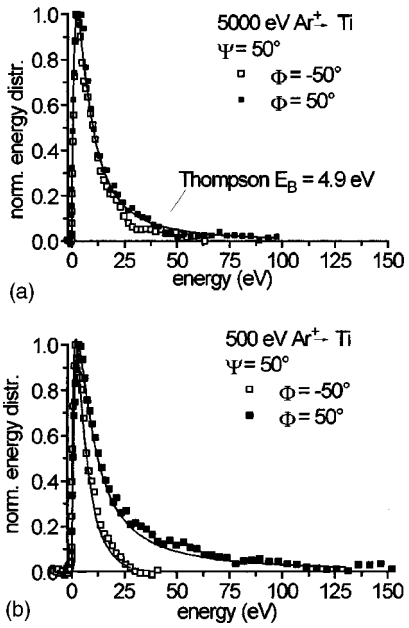

FIG. 6. Influence of the anisotropy on the energy distribution for oblique incidence at high energy (a) and lower energy (b). Open symbols refer to the backward direction; solid symbols refer to the forward direction. In (a) the Thompson distribution with $E_b = 4.9$ eV (heat of sublimation) is depicted for comparison. The solid lines depicted in (b) are calculated according to Eq. (7b) ($\lambda_x = 0.03$; $\lambda_y = 0.25$).

expected to influence the shape of the energy distribution more strongly for grazing emission: the bombardment induces the development of inclined microscopic surfaces, each obeying a forward scattering geometry which leads for oblique exit angles (with respect to the target normal) to a higher mean energy of the sputtered atoms (see below).

The angular variation of the energy distribution is much more pronounced even for comparatively high energies at an oblique angle of incidence—a case of practical importance for many technical applications related to thin film deposi-

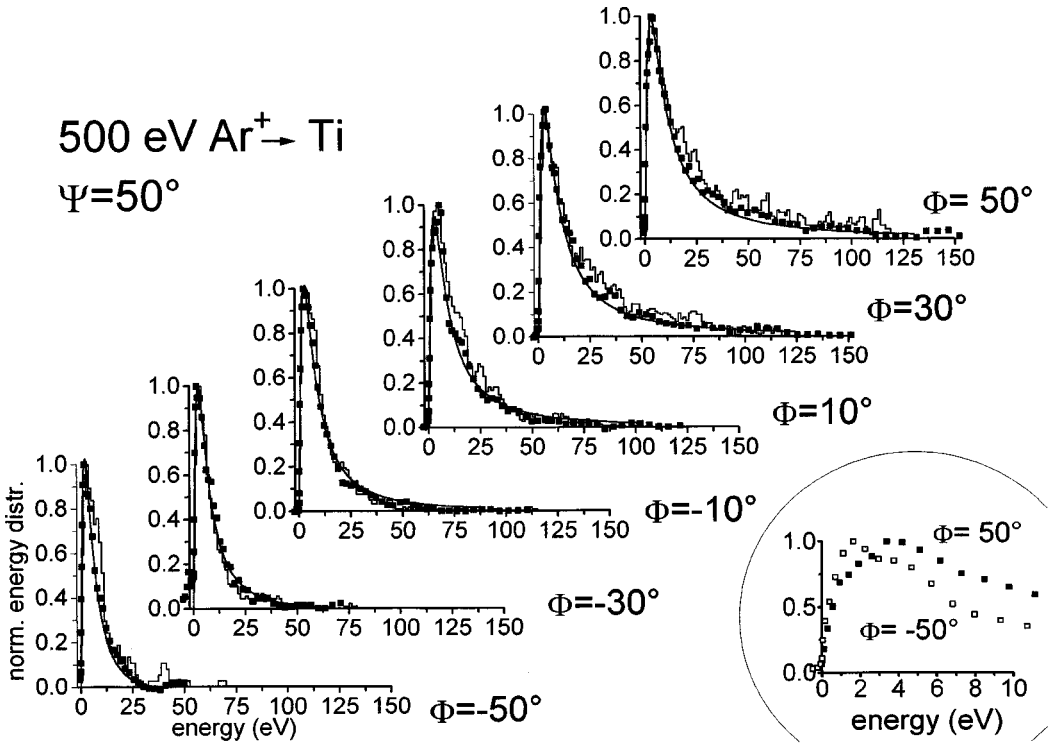

FIG. 7. Set of energy distributions of sputtered titanium atoms at oblique incidence ($\Psi = 50°$) and 500 eV ion energy compared to the TRIM.SP simulation. The solid line depicts the angular variation according to Eq. (7b) ($\lambda_x = 0.03$ and $\lambda_y = 0.25$). The shift of the peak is shown in the inset.

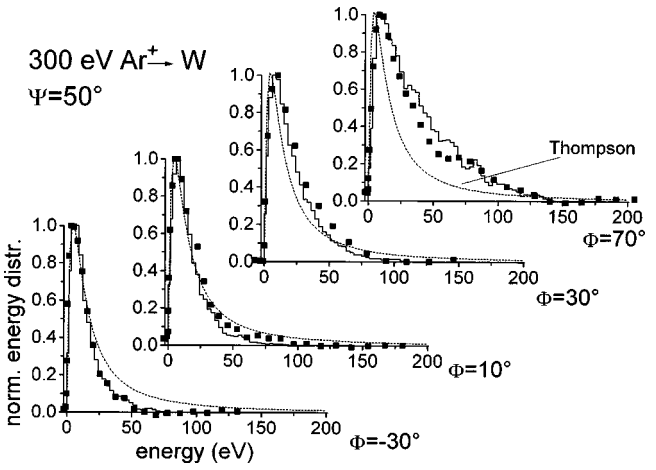

FIG. 8. Energy distributions of tungsten atoms at oblique incidence ($\Psi = 50°$) and 300 eV ion energy compared to the TRIM.SP calculation. The Thompson distribution is added for reference.

tion, since it is well known that the sputtering yield peaks for an angle of incidence typically around $\Psi = 60° - 70°$.[2]

Figure 6 illustrates the behavior of the anisotropy correction of the energy distribution for oblique incidence (argon bombardment of titanium at $\Psi = 50°$) at different bombarding energies for backward ($\Phi = -50°$) and forward emission ($\Phi = +50°$). Whereas at high energy (5000 eV) only minor changes with the emission angle occur [Fig. 6(a)]–indicating

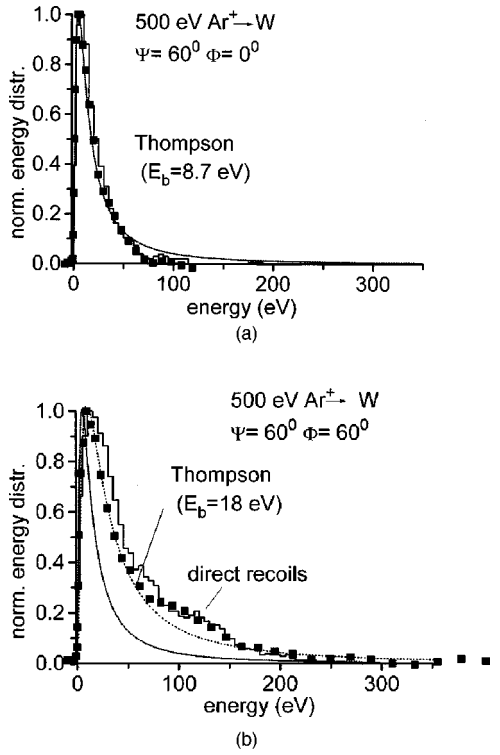

FIG. 9. Energy distribution of tungsten atoms at 500 eV and angle of incidence $\Psi = 60°$: (a) normal emission; (b) forward emission. Note the behavior of the high energy fall-off in comparison to the Thompson-distribution [Eq. (1b)]. The slight hump in the energy distribution in (b) is attributed to direct recoil atoms. In (b) the Thompson distribution with E_b taken as a fitting parameter is included (dotted line).

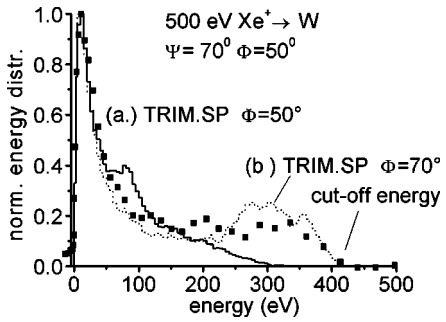

FIG. 10. Energy distribution of sputtered tungsten atoms with xenon bombardment at an angle of incidence of $\Psi = 70°$. The observation direction was $\Phi = 50°$. The simulations shown were calculated for $\Phi = 50°$ (solid stepped curve) and $\Phi = 70°$ (dotted). The cutoff of the energy distribution due to the maximum transferable energy is indicated.

a nearly isotropic recoil distribution inside the solid-pronounced changes for bombardment with 500 eV argon are observed, e.g., a broadening of the energy distribution and a shift of the peak in forward direction [Fig. 6(b)]. The mean energy (obtained from numerical calculation) increases from $\langle E \rangle \simeq 7.4$ eV backward direction to $\langle E \rangle \simeq 30$ eV in forward direction, while the peak shifts from 1.6 eV to 3.4 eV. Note also the change of the energy scale as compared to Fig. 4. The angular variation of the experimental distribution was approximated again by a first order correction of the analytical form of the momentum term, namely

$$\Gamma(E,\Phi) \propto \frac{E}{(E+E_b)^3}\left(1+\lambda_x\sqrt{E\cos\Phi^2+E_b}\pm\lambda_y \sin\Phi\sqrt{E}\right), \tag{7b}$$

where λ_x, λ_y are treated as fitting parameters. The ''+'' and ''−'' signs refer to emission in forward and backward direction, respectively. This dependence describes the set of experimental distributions satisfactorily in the angular range from $\Phi = -70°$ to 50° with the same set of values λ_x, λ_y,

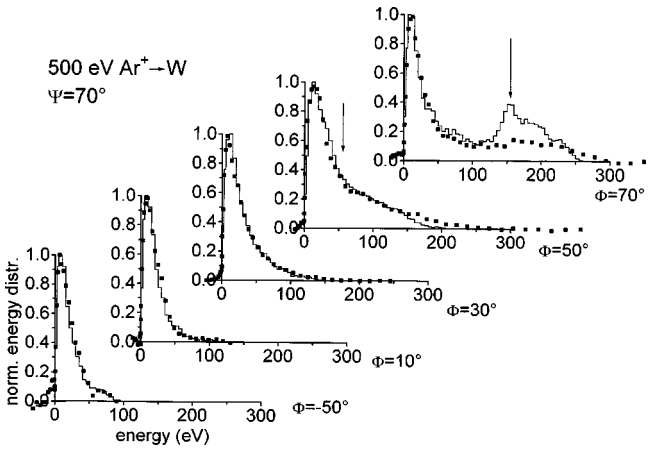

FIG. 11. Systematic change of the energy distributions at oblique incidence $\Psi = 70°$. These measurements were performed using the rotating target device. Influence of direct recoil atoms is visible in the forward direction. The arrows indicate the direct recoil energies.

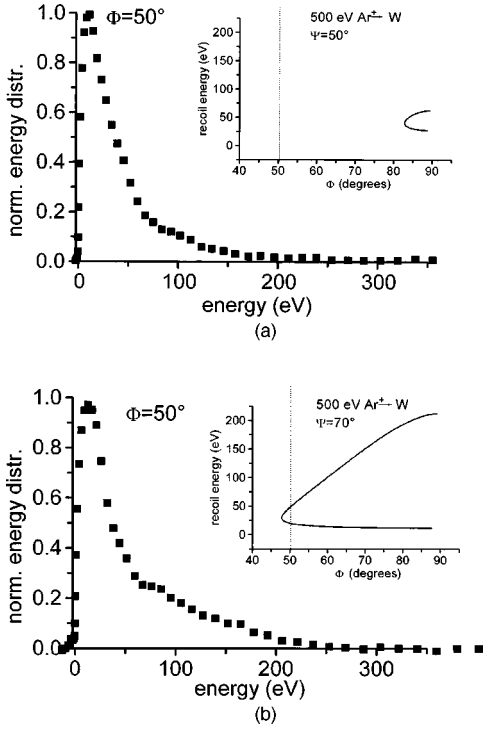

FIG. 12. Influence of direct recoil atoms on the energy spectrum observed at the same emission angle $\Phi = 50°$: (a) angle of incidence 50°; (b) angle of incidence 70°. For case (b) a contribution of direct recoil atoms is expected (see inset).

and E_b taken as the heat of sublimation. The aggreement of the experimental spectra with the TRIM.SP simulation is good (Fig. 7).

Figure 8 shows the result of measurements of sputtered tungsten atoms for an angle of incidence of $\Psi = 50°$ bombarded with 300 eV argon ions together with results of the TRIM.SP simulation and the Thompson distribution [Eq. (1b)] as a reference (dotted lines). The latter is again not an acceptable approximation, and the experimental distributions are systematically shifted in forward direction. Note also the absence of the characteristic E^{-2} falloff.

The energy distributions of the sputtered tungsten atoms become substantially broader at higher bombarding energy: Fig. 9 shows the case of bombardment of tungsten with 500 eV argon ions at an angle of incidence of $\Psi = 60°$. Figure 9(a) shows the distribution for atoms ejected in normal direction ($\Phi = 0$). The ''under-Thompson'' behavior is obvious. This indicates the lack of a sufficient number of high energetic recoil atoms in normal direction. The energy distribution obtained for the forward direction in contrast exhibits a substantial broadening. The attempt to approximate the distribution of Fig. 9(b) by a Thompson type distribution [Eq. (1b)] leads to a value of $E_b = 18$ eV—a factor of 2 higher than the heat of sublimation. Since the broadening is not due to the change of the surface binding energy but due to the anisotropy, one should, therefore, rather speak of a ''Thompson parameter'' E_b, if more general distributions are to be described by a formal expression of this type. The link to the physical picture of a surface binding energy (which is connected to the notion of the atomization heat) is no longer meaningful. The slight hump in the energy distribution of Fig. 9(b) can be explained by the contribution of direct recoil atoms. The good agreement between the experimental data and the results of the TRIM.SP simulation is also remarkable.

The effect of surface roughening is particularly pronounced for bombardment with heavy ions (xenon) at very oblique incidence (70°). Figure 10 shows the measured energy distribution of tungsten atoms together with two TRIM.SP simulations. Case (a) corresponds to an emission angle of $\Phi = 50°$. A discrepancy is obvious especially in the high energy part of the spectrum. The agreement is much better with the simulation (b) which was obtained for $\Phi = 70°$. This observation has lead us to the assumption that the direction of the effective surface normal has changed under the influence of a surface topography induced by the oblique ion bombardment.

We have performed, therefore, further investigations of the influence of direct recoil atoms by using the rotating target device (see Sec. V). We expect that target rotation under oblique bombardment results in a more stationary and smoother surface.[27] The situation for oblique incidence ($\Psi = 70°$) is shown in Fig. 11 along with the TRIM simulations for comparison. Almost no dependence on the emission angle is observed for Φ between $-50°$ and $+30°$, whereas at $+50°$ we observe an onset of substantial broadening. The arrows shown indicate the recoil energies calculated with Eqs. (5a) and (5b). A disagreement between the experiment and the simulation is obvious in the case of extreme forward direction: the direct recoil hump in the simulation appears more pronounced as compared to the measurement. This may be attributed to the residual roughness of the target.

According to the discussion in Sec. IV direct emission is only possible in forward direction for certain angles of incidence. Figure 12 shows the influence of direct recoil atoms on the spectrum. Two experimental spectra for bombardment with 500 eV argon ions with angles of incidence of $\Psi = 50°$ (a) and 70° (b) and for the *same* emission angle $\Phi = 50°$ are compared. At an angle of incidence of $\Psi = 50°$ there should be no direct recoil emission into the selected angle of emission, whereas for $\Psi = 70°$ the critical emission angle is roughly 50°. In this latter case we clearly observe an additional broadening which is not found for bombardment under $\Psi = 50°$.

VII. SUMMARY AND CONCLUSION

Laser induced fluorescence diagnostics is applied in this study to the investigation of energy distributions of sputtered metal atoms (tungsten and titanium) under various conditions of bombardment and particle emission.

For normal incidence and keV bombardment the predictions of the standard linear cascade theory are verified to a good degree of approximation. In the case of sputtering of tungsten values for the surface binding energy are found which slightly exceed the values published for the sublimation heat. With decreasing energy of the ions the measured distributions exhibit increasing deviations from the standard linear cascade theory especially in high energy tail; this behavior is also reproduced by the TRIM.SP simulation. For energies smaller than 500 eV the energy spectra according to the formulation of Falcone approximates the experimental

energy distributions quite well. At normal incidence only weak changes of the distributions with the angle of emission were found for tungsten. For bombardment of titanium by argon ions at lower energy (<500 eV) an increasing broadening of the energy distribution with oblique emission angle and a peak shift towards higher energy was observed in contrast. This angular dependent broadening is explained by the single knock-on sputtering mechanism.

At oblique incidence considerable deviations of the energy distribution as a function of emission angle are observed—in good agreement with the results of the TRIM.SP simulations.

It is possible to approximate the angular variation of the measured distributions by an analytical formula with a fixed value for the surface binding energy (chosen as the heat of sublimation) and one (normal incidence) or two free parameters (oblique incidence). The agreement between experiment and TRIM.SP simulation with bombarding energies as low as 200 eV is generally good with the exception of very oblique emission. The TRIM.SP simulation exhibits in general more details which appear smeared out in the measurement. In particular, structures in the spectra due to direct recoil atoms are much more pronounced in the simulation. The disagreement is attributed mainly to surface roughening not taken into account in the simulation. This is supported by SEM analysis of the targets which typically shows a structure of the sputtered target surface on a μm scale. This work is currently being continued by investigations of sputtered metal films prepared by *in situ* evaporation.

ACKNOWLEDGMENTS

We thank Dr. W. Eckstein (MPI Garching) for leaving the TRIM.SP code to our disposal. Technical support by Carola Fischer is gratefully acknowledged.

[1] *Handbook of Plasma Processing Technology*, edited by I. Rossnagel, S. M. Cuomo, and J. J. Westwood (Noyes Publications, Park Ridge, 1989).
[2] *Secondary Ion Mass Spectroscopy*, edited by A. Benninghoven, F. G. Rüdenhauer, and H. G. Werner (Wiley, New York, 1987).
[3] R. Behrisch, Atom. Plasma Mat. Interact. Data Fusion **1**, 7 (1991).
[4] N. Yoshida, J. Nucl. Mater. **266-269**, 197 (1999).
[5] N. Noda, V. Phillips, and R. Neu, J. Nucl. Mater. **227**, 241 (1997).
[6] W. Hofer, in *Sputtering by Particle Bombardment*, edited by R. Behrisch (Springer, Berlin, 1991), Vol. 3.
[7] W. Berres and H. L. Bay, Appl. Phys. A: Solids Surf. **A33**, 235 (1984).
[8] J. Baxter, G. A. Schick, J. Singh, P. H. Kobrin, and N. Winograd, J. Vac. Sci. Technol. A **4**, 1218 (1986).
[9] M. W. Thompson, Philos. Mag. **18**, 377 (1968).
[10] M. W. Thompson, Phys. Rep. **69**, 335 (1981).
[11] P. Sigmund, in *Sputtering by Particle Bombardment*, edited by R. Behrisch (Springer, Berlin, 1981), Vol. 1.
[12] P. Sigmund, Phys. Rev. **184**, 383 (1969).
[13] P. Sigmund, Rev. Roum. Phys. **17**, 1079 (1972).
[14] J. Lindhard, V. Nielsen, and M. Scharff, Mat. Fys. Medd. K. Dan. Vidensk. Selsk. **33**, No. 14 (1963).
[15] J. B. Sanders, thesis, Univ. Leiden, 1968.
[16] M. W. Schkerl, P. Sigmund, and M. Vicanek, Mat. Fys. Medd. K. Dan. Vidensk. Selsk. **44**, No. 3, 5 (1996).
[17] M. W. Schkerl, M. Vicanek, and P. Sigmund, Nucl. Instrum. Methods Phys. Res. B **102**, 86 (1995).
[18] L. G. Glazov, Nucl. Instrum. Methods Phys. Res. B **122**, 611 (1997).
[19] L. G. Glazov, J. Phys.: Condens. Matter **7**, 6365 (1995).
[20] U. Littmark and P. Sigmund, J. Phys. D **8**, 241 (1975).
[21] M. Posselt, Nucl. Instrum. Methods Phys. Res. B **36**, 420 (1989).
[22] M. Hou and W. Eckstein, J. Appl. Phys. **71**, 3975 (1992).
[23] W. Eckstein, *Computer Simulations of Ion-Solid Interactions* (Springer, Berlin, 1991).
[24] M. Urbassek, Nucl. Instrum. Methods Phys. Res. B **4**, 356 (1984).
[25] M. Vicanek, thesis, Universität Braunschweig, 1989.
[26] W. Eckstein, Nucl. Instrum. Methods Phys. Res. B **27**, 78 (1987).
[27] A. Zalar, Thin Solid Films **124**, 223 (1985).
[28] E. A. Den Hartog, D. W. Duquette, and J. E. Lawler, J. Opt. Soc. Am. B **4**, 48 (1987).
[29] E. Dullni, Appl. Phys. A: Solids Surf. **A38**, 131 (1987).
[30] W. Demtröder, *Laser Spectroscopy* (Springer, Berlin, 1981).
[31] D. R. Stull and H. Prophet, JANAF-Thermochemical Tables, NBS, NSRDS-NBS 37, DC (1971) (unpublished).
[32] H. L. Bay, W. Berres, and E. Hintz, Nucl. Instrum. Methods Phys. Res. **194**, 555 (1982).
[33] R. A. Brizollara, C. B. Cooper, and T. K. Olson, Nucl. Instrum. Methods Phys. Res. B **35**, 36 (1988).
[34] G. Falcone, Riv. Nuovo Cimento **19**, 1 (1990).
[35] G. Falcone and A. Oliva, Appl. Phys. A: Solids Surf. **A32**, 201 (1983).